How to cite: *Angew. Chem. Int. Ed.* **2025**, *64*, e202500173
doi.org/10.1002/anie.202500173

VIP **Polymer Chemistry** *Very Important Paper*

Liquid Crystal-Engineered Polydimethylsiloxane: Enhancing Intrinsic Thermal Conductivity through High Grafting Density of Mesogens

Haitian Zhang, Yongqiang Guo, Yizhi Zhao, Qiuyu Zhu, Mukun He, Hua Guo, Xuetao Shi, Kunpeng Ruan, Jie Kong, and Junwei Gu**

Abstract: The increasing power and integration of electronic devices have intensified serious heat accumulation, driving the demand for higher intrinsic thermal conductivity in thermal interface materials, such as polydimethylsiloxane (PDMS). Grafting mesogens onto PDMS can enhance its intrinsic thermal conductivity. However, the high stability of the PDMS chain limits the grafting density of mesogens, restricting the improvement in thermal conductivity. This work proposes a new strategy to efficiently introduce mesogens onto PDMS through ring-opening copolymerization of liquid crystal cyclosiloxane and octamethylcyclotetrasiloxane, enhancing the grafting density. The relationship between the grafting density and intrinsic thermal conductivity of liquid crystal polydimethylsiloxane (LC-PDMS) is investigated by nonequilibrium molecular dynamics (NEMD) simulations. Based on the simulation results, LC-PDMS with enhanced intrinsic thermal conductivity is synthesized. When the grafting density of mesogens reaches 77.4 %, its intrinsic thermal conductivity coefficient (λ) increases to 0.56 W/(m·K), showing a 180.0 % improvement over ordinary PDMS (0.20 W/(m·K)). The LC-PDMS also exhibits the low dielectric constant (ε, 2.69), low dielectric loss tangent (tanδ, 0.0027), high insulation performance (volume resistivity, 3.51×10^{13} Ω·cm), excellent thermal stability (heat resistance index, 217.8 °C) and excellent hydrophobicity (water contact angle, 137.4°), fulfilling the comprehensive requirements of advanced thermal interface materials.

[*] H. Zhang, Y. Guo, M. He, H. Guo, X. Shi, K. Ruan, J. Kong, J. Gu
Shaanxi Key Laboratory of Macromolecular Science and Technology, School of Chemistry and Chemical Engineering, Northwestern Polytechnical University, Xi'an, Shaanxi, 710072, P. R. China
E-mail: ruankunpeng@nwpu.edu.cn
nwpugjw@163.com

Y. Zhao, Q. Zhu
Queen Mary University of London Engineering School, Northwestern Polytechnical University, Xi'an, Shaanxi, 710072, P. R. China

J. Gu
Chongqing Innovation Center, Northwestern Polytechnical University, Chongqing, 401135, P. R. China
E-mail: gjw@nwpu.edu.cn

Introduction

The rapid development of modern electronic devices has led to significant heat accumulation in electronic components, threatening their stability and reliability.[1–3] The demand for thermal interface materials (TIMs), which are widely used between electronic components and heat sinks, has sharply increased.[4–5] Polydimethylsiloxane (PDMS) is soft and conforms closely to the surfaces of electronic devices, significantly reducing contact thermal resistance caused by microscopic air gaps.[6] Additionally, PDMS offers excellent thermal stability, flexibility, and electrical insulation properties, making it a crucial kind of materials for TIMs.[7–8] However, PDMS contains long molecular chains and large free volumes, often resulting in significant chain entanglements and lattice defects in its microstructure.[9] These characteristics lead to a lack of coordination between molecular and lattice vibrations, causing severe phonon scattering and a low intrinsic thermal conductivity coefficient (λ) of approximately 0.20 W/(m·K).[10–11] As electronic components become increasingly miniaturized and are operated at higher frequencies, the growing heat management demands render traditional PDMS materials insufficient for meeting the current TIMs' need for efficient thermal conductivity and heat dissipation.[12–13]

Researchers typically enhance the thermal conductivity of PDMS by introducing highly thermally conductive fillers.[14] Zhang et al.[15] prepared Al_2O_3/GNPs/PDMS thermally conductive composites by adding spherical alumina (Al_2O_3) and graphene nanoplatelets (GNPs) into the PDMS matrix. At a 50 wt % mass fraction of Al_2O_3/GNPs, the λ of the composite increased from 0.20 W/(m·K) to 0.51 W/(m·K), while its density rose from 1.1 g/cm^3 to 1.5 g/cm^3. This indicates that, while incorporating highly thermally conductive fillers improves the thermal conductivity of PDMS composites, it also increases its density. Moreover, a high filler content would significantly reduce the mechanical properties of PDMS, limiting its applicability in a broader range of scenarios.[16–18]

Researches have suggested that introducing mesogens onto the molecular structure is an effective method for enhancing the intrinsic thermal conductivity of PDMS.[19] Compared with previously mentioned composite approach, this intrinsic method not only significantly enhances the thermal conductivity but also maintains excellent mechanical properties and electrical insulation of PDMS.[20] Hydrosilylation is a widely used technique for grafting mesogens onto polymethylhydrosiloxane.[21–22] Zheng et al.[23] employed

this method to prepare the intrinsically thermally conductive liquid crystal polydimethylsiloxane (LC-PDMS), achieving a λ of 0.35 W/(m K), a 75 % increase compared to ordinary PDMS (0.20 W/(m K)). However, the low hydrogen content in commercially available polymethylhydrosiloxane limits the number of reaction sites for hydrosilylation, preventing a significant increase in the grafting density of mesogens and thereby limiting the enhancement of intrinsic thermal conductivity of PDMS.[24]

In recent years, ring-opening polymerization has been widely used in the synthesis of high-performance PDMS.[25–26] By precisely controlling the type and feed ratio of cyclosiloxane monomers, ring-opening polymerization enables the introduction of specific functional groups onto the PDMS molecular chain, allowing for fine-tuning of the chain structure and significantly increasing the grafting density of these groups.[27–30] Shi et al.[31] employed ring-opening polymerization to polymerize octaphenylcyclotetrasiloxane and octamethylcyclotetrasiloxane (D_4), successfully preparing PDMS with phenyl groups. When the molar ratio of octaphenylcyclotetrasiloxane to D_4 is 7:3, the grafting density of phenyl rings on the PDMS molecular chain reached 64 %, significantly higher than the grafting density of phenyl groups in PDMS (5 %) prepared by hydrosilylation. Therefore, ring-opening polymerization technology is expected to prepare LC-PDMS with higher grafting densities of mesogens, while avoiding poor chain orientation and uneven distribution caused by incomplete reactions in hydrosilylation. This method will further enhance the intrinsic thermal conductivity of PDMS.[32–33]

Based on this, this work proposes a new strategy for efficiently introducing mesogens onto PDMS by adjusting the ratio of liquid crystal cyclosiloxane (TMCS) and D_4 in the ring-opening polymerization to increase the grafting density of mesogens on LC-PDMS. First, nonequilibrium molecular dynamics (NEMD) simulations are employed to investigate the effect of mesogens' grafting density on the intrinsic thermal conductivity of LC-PDMS.[34] Guided by the simulation results, LC-PDMS with high intrinsic thermal conductivity is successfully synthesized using the ring-opening polymerization method. The effect of the TMCS to D_4 ratio on the thermal conductivity, dielectric, insulation, and thermal stability properties of LC-PDMS is investigated. On this basis, the constitutive relationship between "microscopic grafting density/arrangement of mesogens" and "macroscopic thermal conductivity/heat dissipation performance of materials" is revealed, elucidating the intrinsic thermal conduction mechanism of LC-PDMS and providing the theoretical support and guiding framework for the design and development of intrinsically thermally conductive LC-PDMS.

Results and Discussion

Nonequilibrium Molecular Dynamics Simulations of the Intrinsic Thermal Conductivity of LC-DPMS

To elucidate the relationship between the grafting density of mesogens and the intrinsic thermal conductivity of LC-PDMS, we designed a series of LC-PDMS with varying grafting densities of biphenyl mesogens (10 %, 30 %, 50 %, 70 %, 90 %). Nonequilibrium molecular dynamics (NEMD) simulations were used to explore the correlation between the "microscopic grafting density of mesogens" and the "macroscopic thermal conductivity of materials".[35] This part is aimed to provide theoretical insights and a foundation for subsequent experiments. All simulations were conducted using the CVFF force field, with the energy expression provided in Equation (1).[36]

$$E = E_{bond}(r) + E_{angle}(\theta) + E_{dihedral}(\varphi) \quad (1)$$

First, the constructed model underwent structural optimization and energy minimization.[37] Periodic boundary conditions were applied in all directions, with a box size of 50 Å×25 Å×25 Å. Energy minimization was performed using the "minimize" command in the Large-scale Atomic/Molecular Massively Parallel Simulator (LAMMPS) to eliminate unnecessary interactions and reach the system's lowest energy state.[38] High-temperature relaxation was first performed at 900 K in the NVT ensemble to eliminate nonphysical constraints and local energy minima in the initial structure. This allowed the system to overcome energy barriers through high-temperature thermal motion, accelerating its approach to dynamic equilibrium.[39] The NPT ensemble was then run at 900 K and 1 bar to eliminate nonphysical internal stresses and ensure the system reached equilibrium, reflecting the real environmental density distribution.[40] Finally, room-temperature relaxation was carried out in the NPT ensemble at 300 K and 1 bar to obtain the equilibrium structure at room temperature and atmospheric pressure, providing a reliable initial configuration for subsequent simulations.[40] Figure 1a illustrates the molecular chain movement during relaxation. The system's equilibrium was assessed by analyzing the stability of its density and potential energy.[38]

After the system reached equilibrium, the relaxed material was divided into 50 sections along the heat-transfer direction (x-axis). Both ends are fixed, with the left side designated as the heat source (Source) and the right side as the cold source (Sink), and a stable heat flux was applied using the Langevin heating method (Figure 1b). The system was equilibrated for 5×10^5 fs under the NVE ensemble to maintain dynamic equilibrium. After 5×10^5 fs, the temperature along the conduction direction was recorded, and the resulting energy distribution is shown in Figure 1c. The heat flux density J along the heat transfer direction was calculated using Equation (2):

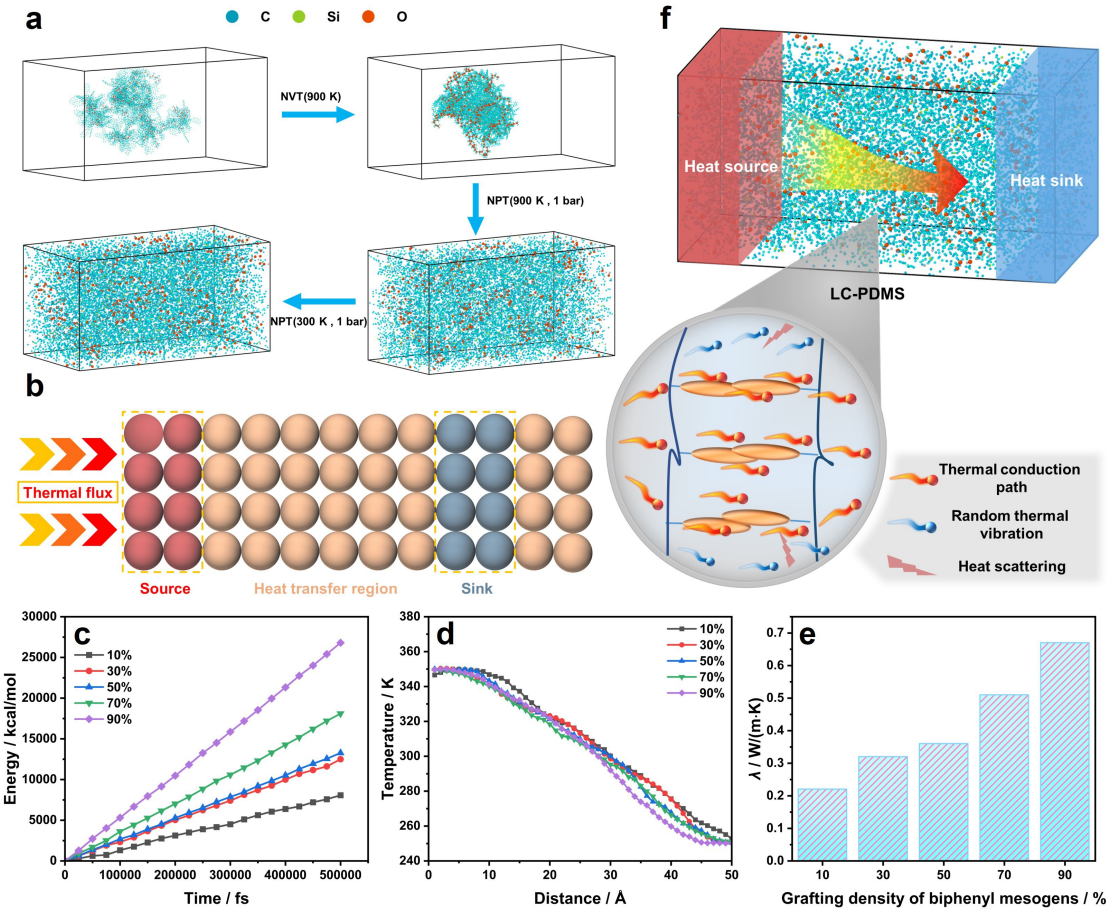

Figure 1. (a) LC-PDMS modeling process during NVT and NPT ensembles. (b) Schematic diagram of NEMD calculation. (c) Absorbed energy curves, (d) temperature distribution curves and (e) intrinsic λ of LC-PDMS. (f) Intrinsic thermal conduction mechanism of LC-PDMS.

$$J = \frac{\partial \mathrm{E}}{\partial t} \qquad (2)$$

$$\nabla T = \frac{\partial \mathrm{T}}{\partial X} \qquad (3)$$

Where J denotes the heat flux density along the heat-transfer direction, E denotes the energy absorbed or emitted by the heat source and cold source, and t denotes the simulation runtime. The slope of the energy-time curve provides the heat flux density J along the heat transfer direction. All five kinds of LC-PDMS systems exhibited stable energy output over 5×10^5 fs, with heat flux density J gradually increasing as the grafting density of biphenyl mesogens increased. When the grafting density of biphenyl mesogens reaches 90 %, the heat flux density J of LC-PDMS is 5.36×10^{12} kcal/mol·s. As the grafting density of biphenyl mesogens increases, the number of these units rises, forming more and stronger π-π stacking interactions. This results in increased energy transfer through the system per unit time, thereby enhancing the heat flux density J.

Figure 1d shows the temperature distribution of the system, with the temperature gradient calculated using Equation (3):

Where ∇T denotes the temperature gradient along the heat-transfer direction, T denotes the temperature, and x denotes the displacement of the heat flux. The slope of the temperature-displacement curve indicates the temperature gradient ∇T along the heat transfer direction. During the 5×10^5 fs period, the temperature in the heat transfer direction of all five kinds of LC-PDMS systems gradually decreases as the heat flux displacement increases. The temperature decreases steadily, indicating stable heat flux output. As the grafting density of biphenyl units in the system increases, the temperature gradient ∇T also increases. When the grafting density of biphenyl mesogens reaches 90 %, the temperature gradient ∇T of the LC-PDMS system is 2.67×10^{10} K/m. This is because, as the grafting density of biphenyl mesogens increases, a higher proportion of larger biphenyl units promotes the formation of a densely packed crystalline structure. The orderly lattice vibrations enhance heat-transfer efficiency, resulting in a larger temperature difference across a fixed heat transfer distance.

Finally, the λ of the system is determined using Fourier's law, as shown in Equation (4):

$$\lambda = -\frac{J}{S\nabla T} \quad (4)$$

Where S denotes the cross-sectional area along the direction of heat transfer. Figure 1e shows the intrinsic λ of LC-PDMS at different biphenyl mesogen grafting densities, calculated using Equation (4). As the biphenyl mesogen grafting density increases, the intrinsic λ of LC-PDMS gradually increases. When the grafting density of biphenyl mesogens reaches 90 %, the λ of LC-PDMS is the highest at 0.67 W/(m K). This increase is due to the significant rise in the number of biphenyl units, which intensifies the π–π stacking interactions between molecules, enhancing local heat conduction and enabling more efficient energy transfer per unit time.[41] Additionally, the increased content of biphenyl mesogens promotes the ordered arrangement of polymer segments, resulting in a highly organized crystalline structure.[42] The densely packed crystalline phases enhance lattice vibrations, improving heat-flow efficiency and significantly increasing the temperature gradient under a fixed heat-transfer distance (Figure 1f). These two mechanisms work synergistically to enhance thermal conductivity. In summary, we investigated the constitutive relationship between the "microscopic grafting density of mesogens" and the "macroscopic λ of materials" using NEMD, demonstrating that increasing grafting density significantly enhances the λ of polymer system. Therefore, by increasing the grafting density of biphenyl mesogens, LC-PDMS with high intrinsic thermal conductivity is expected to be fabricated.

Chemical Structures of LC-PDMS

Based on the above simulation results, we synthesized a biphenyl mesogen-containing polysiloxane (TMCS) and prepared five kinds of intrinsically thermally conductive LC-PDMS with varying grafting densities of mesogens (Table 1) using the ring-opening polymerization method, with D_4 as a co-monomer and self-synthesized tetrabutylammonium oligodimethylsiloxane (TMAS) as the catalyst. The synthesis route is depicted in Figure 2a. During the anionic ring-opening polymerization, OH^- ions from TMAS attack the silicon atoms of TMCS, causing electron cloud redistribution and cleavage of Si-O–Si bonds, which forms an active center for linear polysiloxane oligomers. The active center then attacks other TMCS and D_4, leading to the gradual formation of high-molecular-weight LC-PDMS, as shown in the ring-opening polymerization mechanism[26] in Figure 2b.

Figure S4 shows the ^{1}H nuclear magnetic resonance (^{1}H NMR) spectrum of the intermediate product PTBE, where the characteristic hydrogen peaks of the biphenyl structure are observed at 7.21 ppm, 7.68 ppm, and 8.10 ppm.[42] The multiplet at 2.35 ppm and 2.58 ppm corresponds to the hydrogen atoms on the flexible alkyl chains, while the peaks at 4.88 ppm, 5.13 ppm, and 5.82 ppm correspond to the protons on the terminal vinyl groups of the PTBE structure.[43] Figure S5 shows the ^{1}H NMR spectrum of TMCS, with the characteristic hydrogen peaks of the biphenyl structure appearing at 7.21 ppm, 7.68 ppm, and 8.10 ppm. The multiplets at 0.61 ppm, 1.23 ppm, and 1.64 ppm correspond to the hydrogen atoms on the flexible alkyl chains, while the peak at 0.14 ppm corresponds to the characteristic silicon methyl group on the cyclosiloxane.[44] Figure S6 shows the ^{13}C NMR spectrum of TMCS, where the characteristic carbon peaks of the flexible alkyl chains appear at 15.5 ppm, 25.2 ppm, 28.2 ppm, and 33.2 ppm, while the characteristic carbon peaks of the biphenyl structure appear at 122.1 ppm, 127.9 ppm, and 129.2 ppm.[45] These results confirm the successful grafting of the biphenyl mesogens onto the 1,3,5,7-tetramethylcyclotetrasiloxane. Figure S7 shows the ^{1}H NMR spectrum of the ring-opening polymerization catalyst TMAS, where the characteristic peak of the hydrogen atom on N-CH_3 appears at 3.14 ppm, and the peak of the hydrogen atom on Si-CH_3 appears at 0 ppm.[29] These characterization results confirm the successful synthesis of the intermediate product PTBE, the ring-opening catalyst TMAS, and the liquid crystal cyclosiloxane TMCS.

Figure S8 displays the Fourier transform infrared spectroscopy (FT-IR) spectra of five kinds of LC-PDMS. The characteristic absorption peak of the carbonyl group is observed at 1680 cm^{-1}, that of Si-CH_3 at 1259 cm^{-1}, and the Si–O–Si peaks at 1017 cm^{-1} and 1065 cm^{-1}. Compared to TMCS (Figure S9),[46] the Si-O–Si absorption peaks in LC-PDMS are broader and exhibit a double peak. This behavior, typical of linear polysiloxane, confirms the successful polymerization of TMCS into linear LC-PDMS.

Table 1: Compositions of reaction mixtures and molecular weights of LC-PDMS.[a]

Run	TMCS/D_4/TMAS	Grafting density of biphenyl mesogens[b]/%	M_n[c]/kg mol^{-1}	$Đ$[c]	Product yield[d]/%
1	1:9:0.1	15.7	106.6	2.31	35.2
2	3:7:0.1	33.5	54.6	2.25	86.6
3	5:5:0.1	55.3	48.2	2.04	74.5
4	7:3:0.1	77.4	32.8	1.88	69.7
5	9:1:0.1	44.5	13.7	2.55	11.3

[a] Conditions: TMAS of 0.05 mmol; the base and initiator were mixed firstly in 1 mL of tetrahydrofuran, followed by addition of D_4. [b] Determined by ^{1}H NMR (Figure 2c'). [c] Determined by gel permeation chromatography (GPC) at 20 °C in THF relative to polystyrene standards (Figure 2d). [d] Determined by weight.

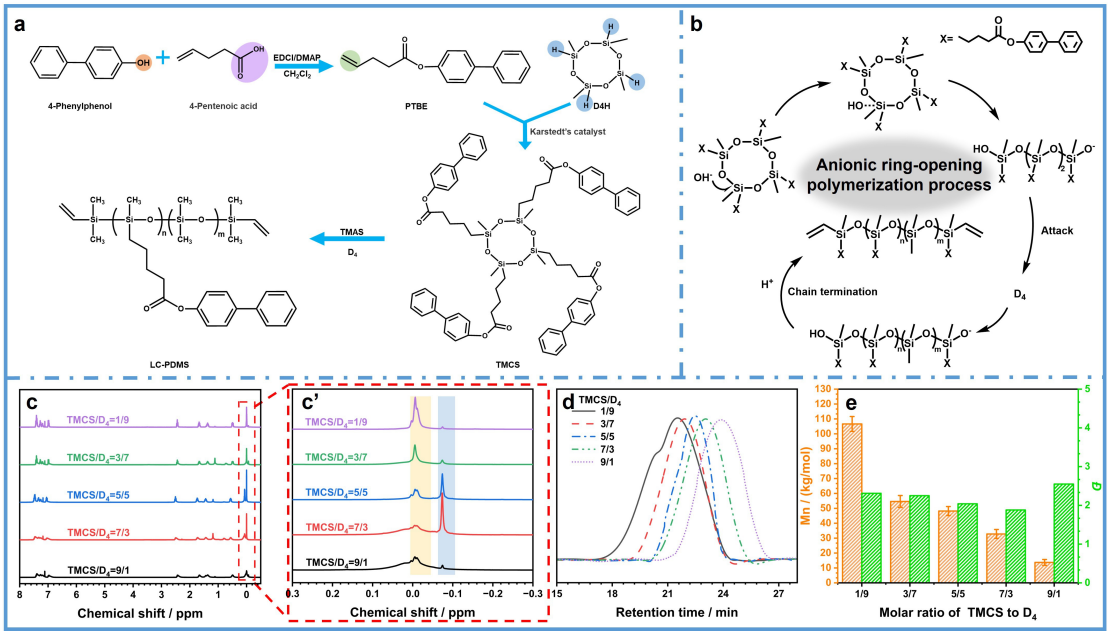

Figure 2. (a) Schematic diagram of the synthesis route for LC-PDMS. (b) Mechanism of anionic ring-opening polymerization. (c) ^{1}H NMR spectra of LC-PDMS and (c') its partially enlarged spectra. (d) Molecular weight distribution curves and (e) corresponding M_n & $Đ$ values of LC-PDMS.

Figures 2c,c' show the ^{1}H NMR spectra of the five kinds of LC-PDMS with magnified views. The characteristic peak of the silicon methyl group in un-grafted mesogens appears at 0 ppm, while that in the grafted units is observed at −0.08 ppm. The proportion of mesogens is determined by calculating the relative intensities of the peaks at 0 ppm and −0.08 ppm. As the TMCS/D_4 ratio increases, the proportion of mesogens in LC-PDMS initially increases, then decreases. The proportion of mesogens in LC-PDMS reaches its maximum at 77.4 % when the TMCS/D_4 ratio is 7/3 (Table 1). Figures 2d,e present the molecular weight distribution curves of the five kinds of LC-PDMS, along with their corresponding number-average molecular weights (M_n) and polydispersity indices ($Đ$). The M_n values of the five kinds of LC-PDMS are 106.6 kg/mol, 54.6 kg/mol, 48.2 kg/mol, 32.8 kg/mol, and 13.7 kg/mol, all corresponding to polymeric molecular weights. As the TMCS/D_4 ratio increases, M_n decreases gradually. The polydispersity indices ($Đ$) of the five kinds of LC-PDMS are all below 2.5, consistent with the characteristics of linear polysiloxane, confirming the successful preparation of LC-PDMS.[47]

The ring-opening reaction mechanism of TMCS and D_4 is further investigated using density functional theory (DFT) analysis, which visualizes the distribution of positive and negative charges on the molecules. Figure S10a presents the electrostatic potential distribution of TMCS after energy minimization using DFT analysis.[48] The positive charge is primarily distributed on the silicon atoms of TMCS, with the silicon atom exhibiting the highest positive potential within the molecule (+1.45 eV). Figure S10b displays the electrostatic potential distribution of D_4 after energy minimization using DFT analysis. The positive charge is predominantly distributed on the silicon atoms of D_4, with the silicon atom exhibiting the largest positive potential within D_4 (+1.36 eV). Furthermore, the positive electrostatic potential of the silicon atoms in TMCS is higher than that of those in D_4, making them more susceptible to attack by OH^- ions and thus promoting the ring-opening reaction. This explains why, at low TMCS/D_4 ratios, the grafting density of biphenyl mesogens in LC-PDMS exceeds the feed ratio. At low TMCS/D_4 ratios, the linear polysiloxane active center preferentially attacks TMCS, leading to a rapid increase in the grafting density of biphenyl mesogens (Figure S11a$_1$). The large biphenyl mesogens introduce significant steric hindrance, which turns the equilibrium of the ring-opening reaction toward the ring structure (Figure S11a$_2$). As a result, the TMCS concentration decreases rapidly, and the active center starts to attack the silicon atoms in D_4, further driving the ring-opening reaction (Figure S11b$_1$). The molecular chains then grow into high-molecular-weight LC-PDMS, eventually reaching equilibrium. As the TMCS/D_4 ratio increases, D_4 is consumed more quickly. The high grafting density of biphenyl mesogens leads to increased steric hindrance, shifting the equilibrium toward the cyclosiloxane (Figure S11b$_2$), which leads to the reduction of the molecular weight. When the TMCS/D_4 ratio reaches 9/1, the D_4 concentration becomes too low, causing the ring-opening reaction to reverse. The proportion of chain transfer and backbiting reactions increases significantly, resulting in the formation of cyclic oligomers through backbiting of the linear polydimethylsiloxane, which reduces the grafting density of biphenyl mesogens in LC-PDMS.

Liquid Crystal Behavior of LC-PDMS

Figure 3a presents the differential scanning calorimetry (DSC) curves of five kinds of LC-PDMS during heating, while Figures $3b_1$–f_3 display the corresponding polarized optical microscopy (POM) images. When the TMCS/D_4 ratio is 9/1, LC-PDMS exhibits two endothermic peaks, corresponding to transitions from the crystalline state to the liquid crystal state, and from the liquid crystal state to the isotropic liquid state. The peak temperatures correspond to the melting temperature (T_m, 21.5 °C) and the clearing point (T_c, 87.4 °C), respectively. Prior to the first endothermic peak, the observed area under POM appears yellow (Figure $3b_1$), indicating that LC-PDMS is anisotropic at room temperature and exists as a semicrystalline compound. As the temperature increases, the POM observation area gradually brightens and becomes more uniform (Figure $3b_2$). After the second endothermic peak, the color of the observed area disappears (Figure $3b_3$), indicating that LC-PDMS exhibits liquid crystallinity but lacks polymer characteristics at this stage.

When the TMCS/D_4 ratio is 7/3 or 5/5, LC-PDMS exhibits three endothermic peaks during heating, corresponding to transitions from the glassy state to the high-elastic state, from the high-elastic state to the liquid crystal state, and from the liquid crystal state to the isotropic liquid state. The peak temperatures correspond to the glass transition temperature (T_g, −19.6 °C and −23.4 °C), melting temperature (T_m, 39.7 °C and 18.8 °C), and clearing point (T_c, 114.5 °C and 84.6 °C), respectively. Before the second endothermic peak appears, the observed area under POM appears yellow (Figures $3c_1, d_1$), indicating that LC-PDMS has anisotropy at room temperature and is a semicrystalline kind of polymers. As the temperature increases, the sample shape changes, and the observed area becomes brighter and more uniform (Figures $3c_2, d_2$), indicating that LC-PDMS exhibits both fluidity and anisotropy, which are characteristic of the liquid crystals. After the third endothermic peak, the color in the observed area gradually disappears (Figures $3c_3, d_3$), indicating that LC-PDMS is in the isotropic liquid state. Moreover, compared to LC-PDMS with a TMCS/D_4 ratio of 5/5, LC-PDMS with a TMCS/D_4 ratio of 7/3 exhibits a higher T_g, a wider liquid crystal range (T_c-T_m), and a larger yellow bright spot region under POM, indicating stronger crystallization ability. At a TMCS/D_4 ratio of 7/3, the grafting density of biphenyl mesogens in the LC-PDMS molecular chain is the highest (77.4 %), and the π–π stacking of rigid biphenyl units promotes the formation of lamellar

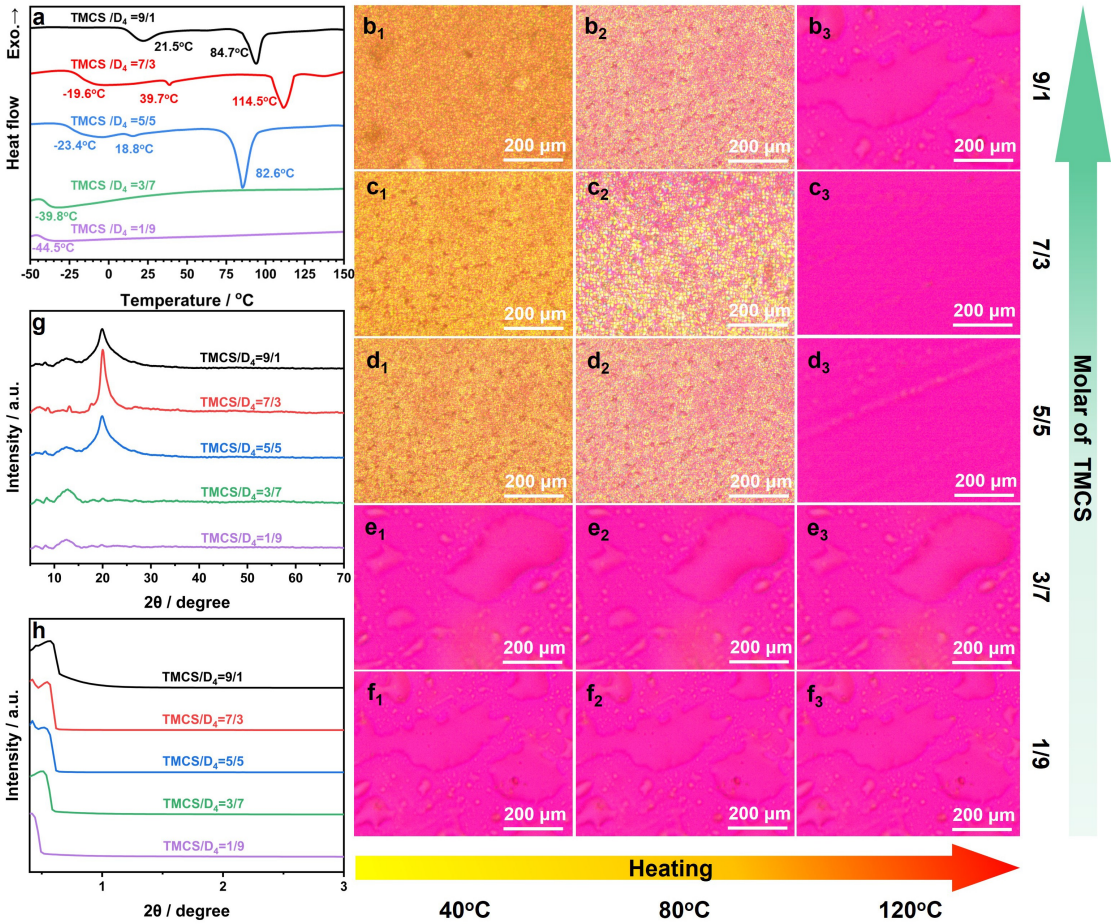

Figure 3. (a) DSC curves, POM images when TMCS/D_4 are (b_1–b_3) 9/1, (c_1–c_3) 7/3, (d_1–d_3) 5/5, (e_1–e_3) 3/7 and (f_1–f_3) 1/9, (g) WAXRD spectra and (h) SAXRD spectra of LC-PDMS.

ordered domains, enhancing crystallization and facilitating the formation of larger crystalline grains. Furthermore, as the TMCS/D_4 ratio increases, the length of the flexible Si-O–Si chains in LC-PDMS decreases, reducing the steric hindrance when the biphenyl units orient, thereby broadening the liquid crystal range.

When the TMCS/D_4 ratio is 1/9 or 3/7, LC-PDMS exhibits only one endothermic peak, corresponding to the transition from the glassy state to the high-elastic state, with peak temperatures at T_g (−44.5 °C and −39.8 °C). This occurs because, at these ratios, the grafting density of biphenyl mesogens on the LC-PDMS molecular chains is low, only 15.7 % and 33.5 %, and the length of the flexible Si-O–Si chains is too large, increasing molecular flexibility and hindering crystallization. Consequently, it exhibits polymer characteristics without liquid crystalline behavior (Figures 3e_1–e_3, f_1–f_3).

Figure 3g shows the WAXRD spectra of the five kinds of LC-PDMS. When TMCS/D_4 = 1/9 and 3/7, LC-PDMS exhibits broad diffraction peaks in the 10°–20° range, indicating an amorphous internal structure.[49] As the TMCS/D_4 ratio increases, LC-PDMS shows a strong diffraction peak at 19.8°, and the intensity of this diffraction peak increases and then decreases with the increasing TMCS/D_4 ratio, indicating the presence of ordered crystal arrangements at the microscopic level. Additionally, the degree of order in the crystal arrangement first increases and then decreases as the TMCS/D_4 ratio increases. When TMCS/D_4 = 7/3, strong diffraction peaks appear near 13.1°, 17.7°, and 19.8°. The diffraction peaks at 13.1° and 17.7° confirm the presence of π–π stacking of biphenyl units in the structure. π–π stacking not only aids in the arrangement and stability of molecules but also enhances the interactions between molecular chains.[50–51] Based on the Scherrer formula ($D = \frac{k\lambda}{B\cos\theta}$, where $k = 0.89$; $\lambda = 0.154$ nm, here λ is the wavelength; B is the half-peak width of the diffraction peaks; θ is the diffraction angle),[52] the grain sizes (D) of LC-PDMS are calculated to be 14.6 nm, 18.0 nm, and 14.1 nm when the TMCS/D_4 ratios are 5/5, 7/3, and 9/1, respectively. This is consistent with the trend of the biphenyl mesogen grafting density in the LC-PDMS structure. According to Bragg's law ($2d\sin\theta = n\lambda$; where $\lambda = 0.154$ nm, here λ is the wavelength; θ is the diffraction angle),[53] when TMCS/D_4 = 7/3, the interplanar spacings (d) of LC-PDMS are 0.47 nm, 0.45 nm, and 0.42 nm. This is because some of the mesogens first self-assemble into crystallites through π–π stacking, and the remaining mesogens further grow around the crystallites, eventually forming spherulites.[54] These spherulites are distributed in ordered microdomains within the microscopic structure. As the grafting density of biphenyl mesogens increases, π–π stacking becomes more likely to occur in the system, and more crystallites form, leading to an increase in the number and size of spherulites and the grain size.

Figure 3h shows the SAXRD spectra of the five kinds of LC-PDMS. When TMCS/D_4 ratios are 5/5, 7/3, and 9/1, LC-PDMS exhibits strong diffraction peaks at $2\theta = 0.715°$, $2\theta = 0.626°$, and $2\theta = 0.774°$, respectively, confirming the formation of highly ordered layered structures within the LC-PDMS. The liquid crystal structure resembles a near-crystalline F phase,[55] with long-range ordered biphenyl stacking structures and larger crystal grains. When TMCS/D_4 = 5/5 and 9/1, the half-peak width of LC-PDMS increases significantly. This increase is attributed to the excess flexible siloxane main chains, which cause entanglement between the chains and disrupt the tight stacking of biphenyl units, reducing the ordering within the polymer system. In contrast, when TMCS/D_4 = 1/9 and 3/7, LC-PDMS does not show strong diffraction peaks. This occurs because, at TMCS/D_4 ratios of 1/9 and 3/7, the proportion of flexible segments in the molecular chains is too high. The increased free volume from larger biphenyl side groups leads to entanglement between molecular chains, hindering the formation of long-range ordered structures and causing LC-PDMS to exhibit isotropic characteristics.

Intrinsic Thermal Conductivity of LC-PDMS

Figure 4a shows the intrinsic λ values of the five kinds of LC-PDMS. As the TMCS/D_4 ratio increases, the intrinsic λ of LC-PDMS initially increases and then decreases. When TMCS/D_4 = 7/3, the intrinsic λ of LC-PDMS reaches its maximum value of 0.56 W/(m K), representing a 180.0 % increase compared to ordinary PDMS (0.20 W/(m K)), and is higher than the λ of LC-PDMS at TMCS/D_4 ratios of 1/9 (0.26 W/(m K)), 3/7 (0.32 W/(m K)), 5/5 (0.45 W/(m K)), and 9/1 (0.41 W/(m·K)). The thermal conduction mechanism in LC-PDMS is predominantly phonon-dominated and heat transfer occurs through phonons. When TMCS/D_4 = 7/3, the grafting density of biphenyl mesogens in the LC-PDMS structure is highest, and the rigid biphenyl units stack to form locally ordered domains, promoting the orderly arrangement of molecular chains into a crystalline structure. The thermal vibration of the neatly arranged lattice causes the phonons to transfer heat with higher efficiency, resulting in higher λ. Additionally, as the grafting density of biphenyl mesogens increases, π–π stacking is more likely to occur. The mesogens can more easily self-assemble crystal nuclei through π–π stacking, and the increased number and size of these nuclei result in larger crystal grain sizes (18.0 nm). This ultimately forms continuous thermal conduction pathways, enhancing phonon transport and resulting in the highest intrinsic λ. When TMCS/D_4 = 5/5 and 9/1, the grafting density of biphenyl mesogens in LC-PDMS is low, the flexible chain length is relatively large, and increased steric hindrance during π–π stacking hinders the formation of ordered domains, reducing molecular chain order.[56] Furthermore, at TMCS/D_4 ratios of 1/9 and 3/7, LC-PDMS does not exhibit liquid crystal properties, resulting in the absence of local ordered structures and increased phonon scattering, which hinders the increase in λ. To simulate the effect of pressure in real working environments on the thermal conductivity of LC-PDMS, the samples were subjected to 2 MPa pressure at 40 °C for 1000 hrs. Figure 4b presents the change in λ of the five kinds of LC-PDMS after 1000 hrs of compression. The change rate of λ in LC-PDMS is below 2 %, indicating its excellent λ stability.

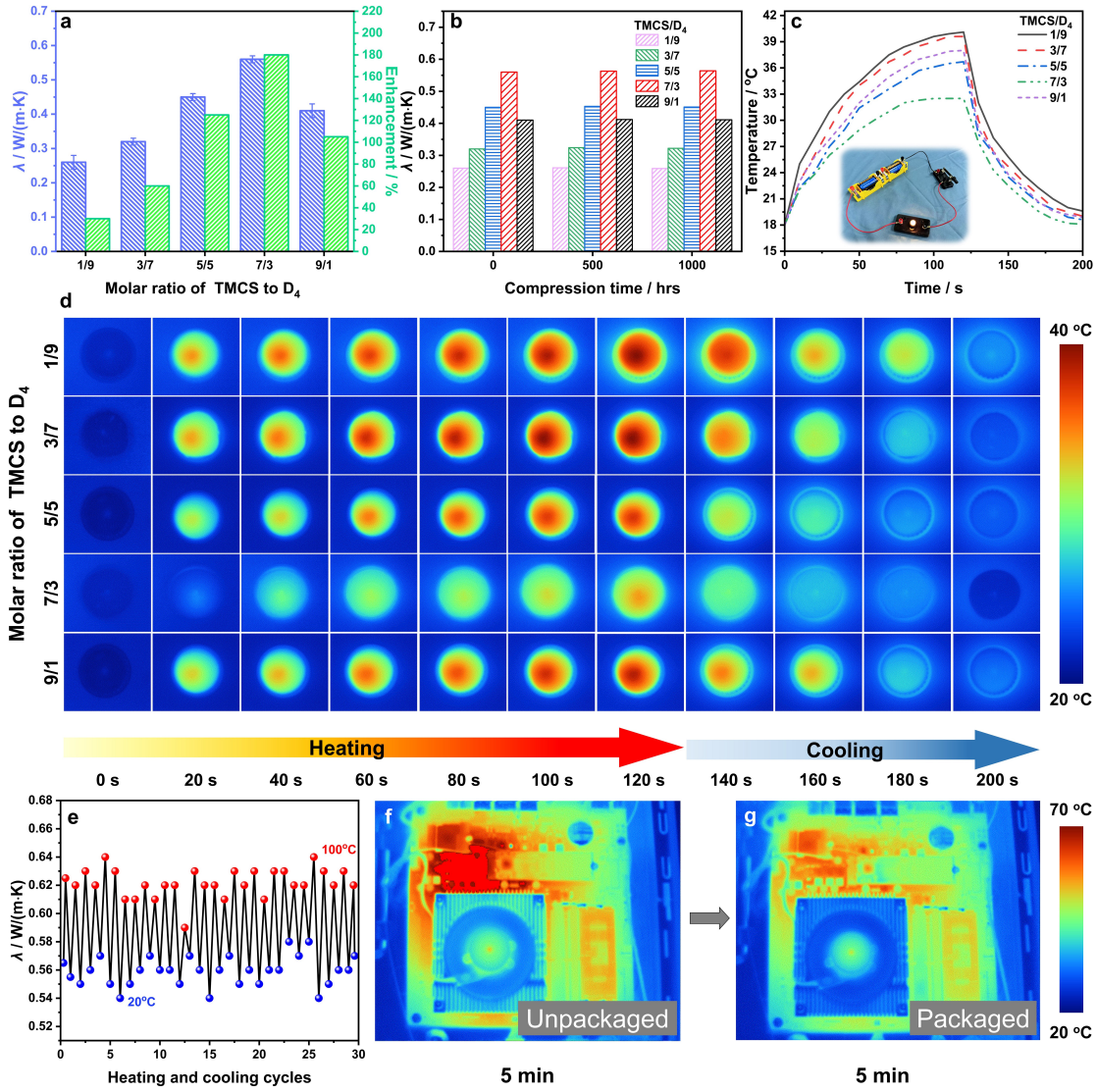

Figure 4. (a) Intrinsic λ of LC-PDMS. (b) Intrinsic λ of LC-PDMS before and after 1000 hrs compression. (c) Relationship curves of temperatures for LC-PDMS vs. time. (d) Infrared thermal images of LC-PDMS. (e) Intrinsic λ of LC-PDMS when TMCS/D_4 are 7/3 during heating & cooling cycles, and infrared images of the motherboard (f) with and (g) without packaging during the overclocking operation stage.

To evaluate the heat dissipation performance of the five kinds of LC-PDMS on irregularly heated device surfaces, LC-PDMS was placed on top of a tungsten filament light bulb. The bulb was powered on at 12 V for 120 seconds, and infrared thermal imaging was employed to monitor the temperature changes at the top of the bulb (Figure 4d). Figure 4c illustrates the relationship between the highest surface temperature of the five kinds of LC-PDMS and the monitoring time. As the bulb operates, the surface temperature of the LC-PDMS gradually increases. At TMCS/D_4 = 1/9, the surface temperature increases the fastest. At TMCS/D_4 = 7/3, the surface temperature of LC-PDMS increases at the slowest rate. Once the temperature stabilized, the temperature at the top of the bulb was recorded. At TMCS/D_4 = 1/9, the surface temperature of LC-PDMS is the highest (43.5 °C), resulting in significant heat accumulation. At TMCS/D_4 = 7/3, the surface temperature of LC-PDMS is the lowest (31.5 °C). After 120 seconds of operation, the power to the bulb was turned off, and the temperature of all LC-PDMS began to decrease. At TMCS/D_4 = 1/9, the surface temperature of LC-PDMS decreases slowly, whereas at TMCS/D_4 = 7/3, LC-PDMS cools rapidly to room temperature. This demonstrates that at TMCS/D_4 = 7/3, LC-PDMS exhibits the best heat dissipation performance, in line with the λ test results above.

Figure 4e shows the changes in the intrinsic λ of LC-PDMS during a "temperature cycling" process from 20 °C to 100 °C when TMCS/D_4 = 7/3. The variation in intrinsic λ does not exceed 0.3 W/(m·K) over 30 cycles at the same temperature, demonstrating that LC-PDMS exhibits stable intrinsic λ and maintains excellent thermal conductivity performance under extreme conditions with frequent temperature fluctuations. Moreover, as the temperature increases, the intrinsic λ of LC-PDMS also increases. With the increase of temper-

ature, LC-PDMS completes the transition from crystalline state to liquid crystal state. In the liquid crystal state, the self-assembly of LC-PDMS can effectively avoid lattice defects and phonon scattering, so that the heat flow can be diffused in the polymer at a higher speed. In addition, higher temperatures accelerate the movement of molecular chains, enhancing phonon-dominated heat transfer efficiency and increasing the intrinsic λ of LC-PDMS. The intrinsic λ of LC-PDMS reaches 0.62 W/(m K) at 100 °C, demonstrating its excellent temperature adaptability and superior thermal conductivity performance at high temperatures.

To evaluate its potential in high-power heating devices, LC-PDMS with the highest intrinsic λ (TMCS/D_4 = 7/3) was placed on an overclocked computer motherboard, and infrared thermal imaging is used to monitor temperature variations during the overclocking phase. Figures 4f–g show infrared thermal images of the computer motherboard during 5 minutes of overclocking, with (Figure 4g) and without (Figure 4f) LC-PDMS, respectively. A darker red indicates higher temperatures and more severe heat accumulation, while blue represents cooler areas. After just 5 minutes of operation, the maximum surface temperature of the computer motherboard reaches 71.4 °C, whereas the maximum surface temperature of the motherboard with LC-PDMS is only 56.3 °C (Figure S12). This demonstrates that LC-PDMS with the highest intrinsic λ minimizes contact thermal resistance and effectively conducts heat from gaps to the heat sink, reducing the temperature of the motherboard and CPU rapidly and preventing heat accumulation, thereby extending the lifespan of electronic devices such as computers.

Electrical and Thermal Properties of LC-PDMS

TIMs are commonly used between electronic components such as chips, power modules, and heat sinks. When these components are operated, they carry current, and if the TIMs lack adequate insulation and electric field stability, current leakage or short circuits may occur, disrupting the normal functioning of electronic devices. Therefore, TIMs must have a low dielectric constant, low dielectric loss, and high resistance to ensure the safety and reliability of electronic components. Figures 5 < a–c show the dielectric properties (dielectric constant ε and dielectric loss tangent tanδ) for the five kinds of LC-PDMS. At a test frequency of 1 MHz, both ε and tanδ of LC-PDMS first increase and then decrease as the TMCS/D_4 ratio increases. When TMCS/D_4 = 7/3, the values of ε and tanδ for LC-PDMS are the lowest, at 2.69 and 0.0027, respectively. This is because the introduction of biphenyl units onto the LC-PDMS molecular structure enhances the polymer's degree of order, effectively reducing electronic and atomic polarization under the influence of the external electric field. Additionally, the larger free volume generated by the bulky side groups significantly weakens dipole polarization. When TMCS/D_4 = 5/5 and 9/1, the proportion of flexible siloxane chains in the LC-PDMS structure is higher, which hinders the formation of biphenyl ordered domains in the liquid crystal phase. This reduces the degree of order in the polymer system and increases electronic and atomic polarization under the external electric field, leading to higher ε and tanδ values.[57] When TMCS/D_4 = 1/9 and 3/7, the relatively large molecular weight of LC-PDMS causes the flexible main chains to entangle and form defects, hindering the close stacking of biphenyl units. This prevents the polymer from maintaining liquid crystallinity, weakens its ability to trap electrons and dipoles, and impedes the migration of bound electrons and

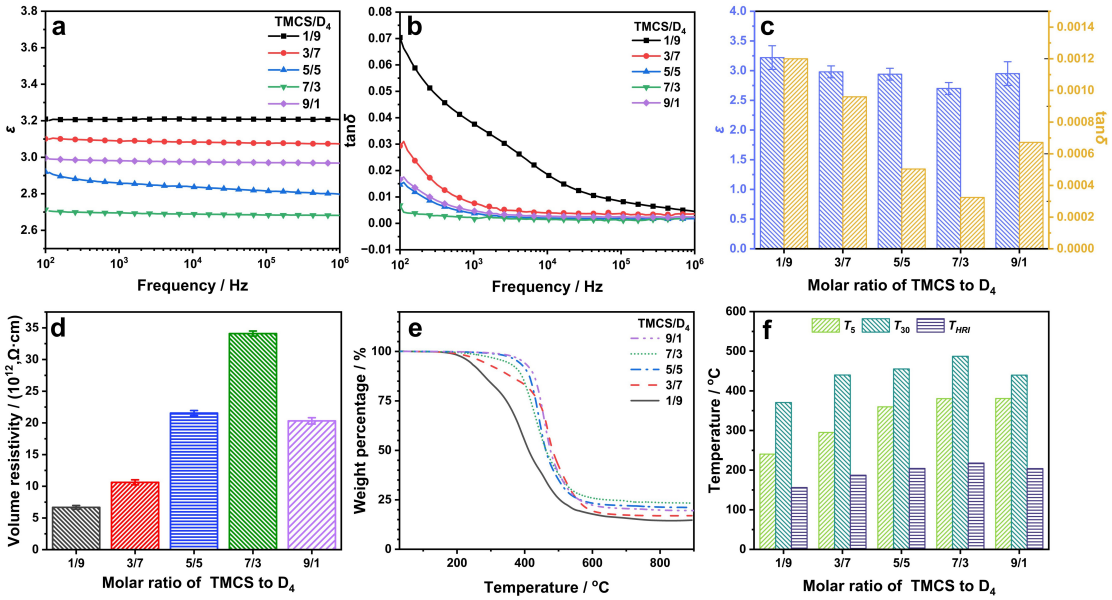

Figure 5. (a) ε and (b) tanδ of LC-PDMS at 10^2–10^6 Hz, (c) ε and tanδ at 10^6 Hz, (d) volume resistivities, (e) TGA curves and (f) characteristic thermal data of LC-PDMS.

dipoles under the external electric field, leading to increased ε and tanδ values.[58–59]

Figure 5d shows the insulating properties of the five kinds of LC-PDMS. The volume resistivity of the five kinds of LC-PDMS is higher than that of commercial RTV-2SR silicone rubber (2.19×10^{12} Ω cm), and increases first before decreasing as the TMCS/D_4 ratio increases. When TMCS/D_4 = 7/3, the volume resistivity of LC-PDMS reaches its peak value of 3.51×10^{13} Ω·cm. This significant increase is primarily due to enhanced π–π stacking between biphenyl units in LC-PDMS, which strengthens the polymer chain's ability to trap charge carriers, effectively inhibiting the migration of free charges and improving insulation performance. When TMCS/D_4 = 5/5 and 9/1, the grafting density of biphenyl mesogens in the LC-PDMS molecular structure decreases, and the longer flexible siloxane chains tend to entangle, hindering the tight stacking of polymer chains. This loose molecular structure reduces volume resistivity, leading to decreased insulation performance.[60–61] When TMCS/D_4 = 1/9 and 3/7, the grafting density of biphenyl mesogens in LC-PDMS decreases further, significantly weakening the interaction between mesogens and disrupting the ordered arrangement of polymer chains, reducing the π–π stacking effect. Meanwhile, the increase in the proportion of flexible siloxane segments exacerbates the random entanglement of polymer chains, hindering their close arrangement and ability to effectively trap charge carriers. These factors combine to significantly reduce volume resistivity, leading to a noticeable decrease in insulation performance.

TIMs must withstand the high temperatures generated during high-power operation of electronic devices for extended periods without decomposition, requiring superior thermal stability. Figure 5e presents the TGA curves of the five kinds of LC-PDMS, with corresponding thermal data in Figure 5f. When TMCS/D_4 = 3/7, 5/5, 7/3, and 9/1, LC-PDMS exhibits similar thermal degradation behavior, with a mass loss of less than 5 % before 285 °C, primarily due to the decomposition of small amounts of unreacted monomers. When TMCS/D_4 = 1/9, the higher proportion of D_4 in the ring-opening polymerization results in a slower copolymerization rate compared to the homopolymerization rate, leading to the formation of small amounts of low-molecular-weight polydimethylsiloxane, which decomposes before 285 °C, causing a mass loss of 15 %. Furthermore, LC-PDMS decomposes rapidly between 200 °C and 600 °C, primarily due to the pyrolytic cleavage of flexible chains, including the breaking of siloxane bonds, cleavage of side-chain segments, and degradation and carbonization of aromatic rings. As the TMCS/D_4 ratio increases, the thermal heat resistance index (T_{HRI}, $T_{HRI} = 0.49\times[T_5 + 0.6\times(T_{30} - T_5)]$,[62] where T_5 and T_{30} are corresponding decomposition temperatures of 5 wt % and 30 wt % weight loss, respectively) of LC-PDMS first increases and then decreases. When TMCS/D_4 = 7/3, LC-PDMS achieves the highest T_{HRI} value of 217.8 °C, surpassing that of LC-PDMS with TMCS/D_4 = 1/9 (156.1 °C), 3/7 (187.2 °C), 5/5 (204.3 °C), and 9/1 (203.9 °C), and also has the highest char residue (27.5 %). This is because, as the TMCS/D_4 ratio increases, the grafting density of biphenyl mesogens in the LC-PDMS molecular chain first increases and then decreases. When TMCS/D_4 = 7/3, the grafting density of biphenyl mesogens reaches its maximum (77.4 %), and at this point, more biphenyl units in the molecular structure promote the formation of π–π stacking, enhancing intermolecular interactions and effectively restricting molecular thermal motion, thereby imparting superior thermal stability.

Conclusions

This work proposes a new strategy to efficiently introduce mesogens onto PDMS by copolymerizing liquid crystal cyclosiloxane with octamethylcyclotetrasiloxane, thereby increasing the grafting density of mesogens. Firstly, NEMD calculations are performed to confirm that increasing the grafting density of mesogens significantly enhances the thermal conductivity of LC-PDMS. Based on the simulation results, LC-PDMS is then synthesized through the ring-opening polymerization of TMCS and D_4. At a TMCS/D_4 ratio of 7/3, the proportion of mesogens in the LC-PDMS molecular chains reaches its maximum (77.4 %), resulting in optimal thermal conductivity, with an intrinsic λ of 0.56 W/(m·K). Meanwhile, at 1 MHz, LC-PDMS exhibits ε and tanδ values of 2.69 and 0.0027, respectively, while also providing excellent insulating properties (volume resistivity = 3.51×10^{13} Ω cm), thermal stability (T_{HRI} = 217.8 °C), and hydrophobicity (θ = 137.4°). This makes it ideal for use as a TIM between electronic components and heat sinks, addressing local heat accumulation. These properties make LC-PDMS highly suitable for applications in advanced flexible electronics and wearable devices. This work offers a detailed analysis of how the grafting density of mesogens influences the thermal conductivity of polydimethylsiloxane. It also simulates and discusses the ring-opening polymerization kinetics of various cyclosiloxanes, providing valuable insights for the preparation and practical application of thermally conductive liquid crystal polydimethylsiloxane.

Acknowledgements

The authors are grateful for the support from the National Natural Science Foundation of China (52473083, 52403114), the support and funding from National Scientific Research Project (Basis Strengthening Plan), Natural Science Basic Research Program of Shaanxi (2024JC-TBZC-04), Shaanxi Province Key Research and Development Plan Project (2023-YBGY-461), the Innovation Capability Support Program of Shaanxi (2024RS-CXTD-57), the Foundation of Aeronautics Science Fund (2024Z054053002), Natural Science Foundation of Chongqing, China (2023NSCQ-MSX2547), Fundamental Research Funds for the Central Universities (D5000240067, D5000240077), Innovation Foundation for Doctor Dissertation of Northwestern Polytechnical University (CX2024094), Undergraduate Innovation & Business Program in Northwestern Polytechnical University (202410699230), the Analytical & Testing Center

of Northwestern Polytechnical University for XRD, DSC and TGA tests performed in this work.

Conflict Of Interest

The authors declare no conflict of interest.

Data Availability Statement

The data that support the findings of this study are available from the corresponding authors upon reasonable request.

Keywords: ring-opening polymerization · intrinsic thermal conductivity · polydimethylsiloxane · liquid crystals · grafting density

[1] G. Q. Li, S. H. Liu, Z. W. Xu, J. H. Guo, S. Y. Tang, X. Ma, *Soft Sci.* **2023**, *3*, 37.
[2] Y. X. Han, K. P. Ruan, X. Y. He, Y. S. Tang, H. Guo, Y. Q. Guo, H. Qiu, J. W. Gu, *Angew. Chem. Int. Ed.* **2024**, *63*, e202401538.
[3] Z. Y. Yuan, H. Q. Ma, M. A. Hussien, Y. K. Feng, *Macromol. Mater. Eng.* **2021**, *306*, 2100428.
[4] P. Q. Cai, B. H. Hu, W. R. Leow, X. Y. Wang, X. J. Loh, Y. L. Wu, X. D. Chen, *Adv. Mater.* **2018**, *30*, 1800572.
[5] X. D. Zhang, G. Yang, B. Y. Cao, *Adv. Mater. Interfaces* **2022**, *9*, 2200078.
[6] M. K. He, X. Zhong, X. H. Lu, J. W. Hu, K. P. Ruan, H. Guo, Y. L. Zhang, Y. Q. Guo, J. W. Gu, *Adv. Mater.* **2024**, *36*, 10.1002/adma.202410186.
[7] H. Zhang, W. You, F. Bian, W. Yu, *Macromolecules* **2022**, *55*, 8834–8845.
[8] B. Yi, S. Wang, C. Hou, X. Huang, J. Cui, X. Yao, *Chem. Eng. J.* **2021**, *405*, 127023.
[9] J. Y. Yu, Y. Z. Liu, *Angew. Chem. Int. Ed.* **2017**, *56*, 8706–8710.
[10] Y. G. Ji, Z. B. Wen, J. F. Fan, X. L. Zeng, X. L. Zeng, R. Sun, L. L. Ren, *Compos. Sci. Technol.* **2023**, *231*, 109840.
[11] X. X. He, Z. Y. He, Q. S. Zuo, Y. Ma, J. P. Zhang, L. J. Li, S. Y. Wu, Y. Chen, Y. Luo, *Compos. Sci. Technol.* **2024**, *252*, 110625.
[12] Z. A. Zhang, Z. B. Wen, J. S. Sheng, C. Zeng, J. F. Fan, L. L. Ren, X. L. Zeng, R. Sun, P. Chen, *Chem. Eng. J.* **2024**, *495*, 153352.
[13] H. T. Yu, Y. Y. Feng, L. Gao, C. Chen, Z. X. Zhang, W. Feng, *Macromolecules* **2020**, *53*, 7161–7170.
[14] J. M. Wei, M. Z. Liao, A. J. Ma, Y. P. Chen, Z. H. Duan, X. Hou, M. H. Li, N. Jiang, J. H. Yu, *Compos. Commun.* **2020**, *17*, 141–146.
[15] Y. C. Zhang, W. Yu, L. Y. Zhang, J. S. Yin, J. K. Wang, H. Q. Xie, *J. Therm. Sci. Eng. Appl.* **2018**, *10*, 011014.
[16] Y.-T. Li, W.-J. Liu, F.-X. Shen, G.-D. Zhang, L.-X. Gong, L. Zhao, P. Song, J.-F. Gao, L.-C. Tang, *Composites Part B* **2022**, *238*, 109907.
[17] H. Y. Zhu, S. X. Wu, R. Tang, Y. Li, G. Chen, B. X. Huang, B. Y. Peng, *Polymer* **2024**, *16*, 1491.
[18] Y. Zhang, S. Yang, Y. L. Liu, T. Gu, F. Liu, *J. Mater. Chem. A* **2024**, *12*, 27527–27539.
[19] Y. Li, P. Pan, C. Liu, W. Y. Zhou, C. G. Li, C. D. Gong, H. L. Li, L. Zhang, H. Song, *J. Polym. Eng.* **2020**, *40*, 573–581.
[20] Y. H. Zhang, X. X. Wang, W. L. Yang, H. X. Yan, X. Y. Zhang, D. X. Han, Y. F. He, C. S. Li, L. G. Sun, *Molecules* **2023**, *28*, 4858.
[21] C. Sharma, N. Pandya, G. Desai, Y. Agrawal, *React. Funct. Polym.* **2024**, *202*, 106009.
[22] Y. C. Wu, P. Wang, *Angew. Chem. Int. Ed.* **2022**, *61*, e202205382.
[23] X. L. Zheng, Y. J. Zhan, Y. C. Liu, M. P. Lu, E. X. Jiao, H. Z. Zhang, J. Shi, M. G. Lu, K. Wu, *Polym. Chem.* **2022**, *13*, 3915–3929.
[24] C. S. Li, Y. Liu, C. W. Lo, H. R. Jiang, *Soft Matter* **2011**, *7*, 7511–7516.
[25] L. Shi, A. Boulegue-Mondiere, D. Blanc, A. Baceiredo, V. Branchadell, T. Kato, *Science* **2023**, *381*, 1011–1014.
[26] K. Fuchise, K. Sato, M. Igarashi, *Macromolecules* **2021**, *54*, 5204–5217.
[27] E. Perju, E. Cuervo-Reyes, S. Shova, D. M. Opris, *RSC Adv.* **2018**, *8*, 7569–7578.
[28] K. Fuchise, M. Igarashi, K. Sato, S. Shimada, *Chem. Sci.* **2018**, *9*, 2879–2891.
[29] A. Zlatanic, D. Radojcic, X. M. Wan, J. M. Messman, P. R. Dvornic, *Macromolecules* **2017**, *50*, 3532–3543.
[30] K. Matsumoto, Y. Oba, Y. Nakajima, S. Shimada, K. Sato, *Angew. Chem. Int. Ed.* **2018**, *57*, 4637–4641.
[31] J. F. Shi, N. Zhao, S. Xia, S. F. Liu, Z. B. Li, *Polym. Chem.* **2019**, *10*, 2126–2133.
[32] S. Huang, L. Han, H. W. Ma, L. Lei, R. X. Zhang, H. Y. Shen, L. C. Yang, C. Li, S. B. Zhang, Y. Li, *Polym. Chem.* **2020**, *11*, 2559–2567.
[33] Z. Y. Kuang, Y. J. Fan, L. Tao, M. L. Li, N. Zhao, P. Wang, E. Q. Chen, F. Fan, H. L. Xie, *ACS Appl. Mater. Interfaces* **2018**, *10*, 27269–27277.
[34] A. Albaugh, T. R. Gingrich, *Nat. Commun.* **2022**, *13*, 2204.
[35] Y. Q. Yan, Y. C. Tao, C. K. Liang, Z. X. Liu, T. Li, G. M. An, *Langmuir* **2024**, *40*, 22037–22048.
[36] A. Vasilev, T. Lorenz, C. Breitkopf, *Polymer* **2022**, *14*, 2046.
[37] X. J. Liu, C. P. Lin, Z. H. Rao, *Int. J. Therm. Sci.* **2021**, *159*, 106646.
[38] M. Mohammadi, H. Fazli, M. Karevan, J. Davoodi, *Eur. Polym. J.* **2017**, *91*, 121–133.
[39] S. Plimpton, *J. Comput. Phys.* **1995**, *117*, 1–19.
[40] J. Castillo-Tejas, S. Carro, O. Manero, *ACS Macro Lett.* **2017**, *6*, 190–193.
[41] X. R. Fan, Z. Liu, S. S. Wang, J. W. Gu, *Susmat* **2023**, *3*, 877–893.
[42] F. Y. Zhang, J. L. Zhang, K. Zhang, X. Zhong, M. K. He, H. Qiu, J. W. Gu, *Adv. Sci.* **2024**, 10.1002/advs.202410362.
[43] P. Gerdt, A. Studer, *Angew. Chem. Int. Ed.* **2022**, *61*, e202206964.
[44] H. Zhu, T. J. Buchtal, M. Mitsuishi, *Appl. Surf. Sci.* **2021**, *563*, 150245.
[45] T. Ube, T. Ikeda, *Angew. Chem. Int. Ed.* **2014**, *53*, 10290–10299.
[46] M. Yoshikawa, Y. Tamura, R. Wakabayashi, M. Tamai, A. Shimojima, K. Kuroda, *Angew. Chem. Int. Ed.* **2017**, *56*, 13990–13994.
[47] P. P. Hu, J. Madsen, A. L. Skov, *Nat. Commun.* **2022**, *13*, 370.
[48] C. H. Li, C. Wang, C. Keplinger, J. L. Zuo, L. Jin, Y. Sun, P. Zheng, Y. Cao, F. Lissel, C. Linder, X. Z. You, Z. A. Bao, *Nat. Chem.* **2016**, *8*, 619–625.
[49] S. S. Xu, J. Zhou, P. J. Pan, *Prog. Polym. Sci.* **2023**, *140*, 101676.
[50] R. Yang, L. Ding, W. Chen, L. Chen, X. Zhang, J. Li, *Macromolecules* **2017**, *50*, 1610–1617.
[51] W. L. Chen, K. Wu, Z. Y. Tan, M. G. Lu, *Polym. Int.* **2020**, *69*, 346–354.

[52] K. D. Khalil, S. M. Riyadh, N. S. Alkayal, A. H. Bashal, K. H. Alharbi, W. Alharbi, *Polymer* **2022**, *14*, 2827.
[53] T. Giang, J. Kim, *J. Electron. Mater.* **2017**, *46*, 627–636.
[54] K. P. Ruan, J. W. Gu, *Macromolecules* **2022**, *55*, 4134–4145.
[55] Q. Zhang, G. K. Chen, K. Wu, J. Shi, L. Y. Liang, M. G. Lu, *J. Appl. Polym. Sci.* **2020**, *137*, e49143.
[56] K. P. Ruan, X. T. Shi, Y. L. Zhang, Y. Q. Guo, X. Zhong, J. W. Gu, *Angew. Chem. Int. Ed.* **2023**, *62*, e202309010.
[57] J. Duan, C. Mei, W. Wu, L. Rao, H. Fan, Y. Tang, A. Zhang, *Macromolecules* **2021**, *54*, 6947–6955.
[58] J. Lu, Y. Zhang, J. Li, M. Fu, G. Zou, S. Ando, Y. Zhuang, *Macromolecules* **2023**, *56*, 2164–2174.
[59] J. J. Huang, X. D. Zhang, R. X. Liu, Y. H. Ding, D. J. Guo, *Nat. Commun.* **2023**, *14*, 1483.
[60] J. A. Zhang, H. Wang, T. X. Zhang, X. Y. Sun, Y. Meng, C. Q. Ma, T. Y. Zhang, N. Lu, C. Liu, Y. Zeng, *Compos. Sci. Technol.* **2023**, *233*, 109915.
[61] R. D. Bhatt, J. P. Patel, P. H. Parsania, *J. Polym. Mater.* **2024**, *39*, 37–53.
[62] S. Pal, B. Rai, A. K. Tyagi, S. Rattan, V. Kumar, *J. Polym. Mater.* **2024**, *39*, 55–70.

Manuscript received: January 3, 2025
Accepted manuscript online: January 20, 2025
Version of record online: January 28, 2025